Novel luminescent benzopyranothiophene- and BODIPY-derived aroylhydrazonic ligands and their dicopper(II) complexes: syntheses, antiproliferative activity and cellular uptake studies

Jesica Paola Rada, Jérémy Forté, Geoffrey Gontard, Claude-Marie Bachelet, Nicolás Rey, Michèle Salmain, Vincent Corcé

Novel luminescent benzopyranothiophene- and BODIPY-derived aroylhydrazonic ligands and their dicopper(II) complexes: syntheses, antiproliferative activity and cellular uptake studies

Jesica Paola Rada,[a] Jérémy Forté,[b] Geoffrey Gontard,[b] Claude-Marie Bachelet, [c] Nicolás A. Rey,*[a] Michèle Salmain[b] and Vincent Corcé*[b]

[a] *Dr. J. P. Rada, 0000-0003-4344-2469; Dr. N. A. Rey, 0000-0002-0624-7560*
LABSO-Bio Laboratory, Department of Chemistry
Pontifical Catholic University of Rio de Janeiro
Rua Marquês de São Vicente, 225, 22453-900 Rio de Janeiro (Brazil)
E-mail: nicoarey@puc-rio.br

[b] *J. Forté, 0000-0002-9363-4162; G. Gontard, 0000-0002-4099-5423;*
Dr. V. Corcé, 0000-0003-2481-7608; Dr. M. Salmain, 0000-0003-3039-5659
Institut Parisien de Chimie Moléculaire (IPCM)
Sorbonne Université, CNRS
4 place Jussieu, 75005 Paris (France)
E-mail: vincent.corce@sorbonne-univesite.fr

[c] *Dr C-M. Bachelet, Plateforme ICM.Quant, Hôpital de la Pitié-Salpêtrière, Inserm U1127, CNRS UMR 7225, Sorbonne Université, 75013 Paris, (France)*

Abstract

Two novel unsymmetrical binucleating aroylhydrazonic ligands and four dicopper(II) complexes carrying fluorescent benzopyranothiophene (BPT) or boron dipyrromethene (BODIPY) entities were synthesized and fully characterized. Complex **3**, derived from the BPT-containing ligand **H_3L1**, had its crystal structure elucidated through X-ray diffraction measurements. The absorption and fluorescence profiles of all the compounds obtained were discussed. Additionally, the stability of the ligands and complexes was monitored by UV-visible spectroscopy in DMSO and biologically relevant media. All the compounds showed moderate to high cytotoxicity towards the triple negative human breast cancer cell line MDA-MB-231. BPT derivatives were the most cytotoxic, specially **H_3L1**, reaching an IC_{50} value up to the nanomolar range. Finally, fluorescence microscopy imaging studies employing mitochondria- and nucleus-staining dyes showed that the BODIPY-carrying ligand **H_3L2** was highly cell permeant and suggested that the compound preferentially accumulates in the mitochondria.

Keywords:
aroylhydrazones; copper complexes; anticancer agents; cytotoxicity; cellular uptake

1. Introduction

Copper constitutes an essential element[1], being involved in many important biological processes[2]. Also, many synthetic mono- and polynuclear copper complexes display potential pharmacologically relevant properties, like the ability to interact with DNA and induce its cleavage by hydrolysis of the phosphodiester bonds or oxidation[3, 4].

Numerous copper complexes show high *in vitro* antiproliferative activity and, from this broad set of compounds, a few rules were delineated regarding the most appropriate geometries and oxidation states, desirable for an enhanced cytotoxicity[5]. Among the most promising ligands examined, tridentate aroylhydrazones (Figure 1) afford mono-, di- or tetranuclear copper complexes by coordination through their O,N,O systems. Cytotoxicity of the complexes towards several cancer cell lines was demonstrated *in vitro* [6], some of them showing a good selectivity with respect to healthy cells[7, 8] and much higher activity than that of the free ligands[9-12].

As part of a wide research program initially aimed at the design of synthetic mimics for dinuclear metalloenzymes such as catechol oxidase, a type-3 copper enzyme, some of us introduced several new binucleating Schiff-base ligands whose dicopper(II) complexes exhibited significant nuclease activity[13, 14]. More recently, we reported the synthesis of several unsymmetrical binucleating ligands comprising of an aroylhydrazone moiety and a N,N,N or N,N,O tridentate pendant arm joined together by a central 4-methylphenol ring (BPMAMFF-Hz and HBPAMFF-Hz in Figure 1) and their dicopper(II) complexes[15, 16]. The biological properties of the ligands and complexes were extensively studied and revealed that the complexes derived from the HBPAMFF-Hz ligands were highly cytotoxic towards the triple negative breast cancer cell line MDA-MB-231, whereas the ones containing the ligand BPMAMFF-Hz were virtually inactive (IC_{50} > 10 µM).

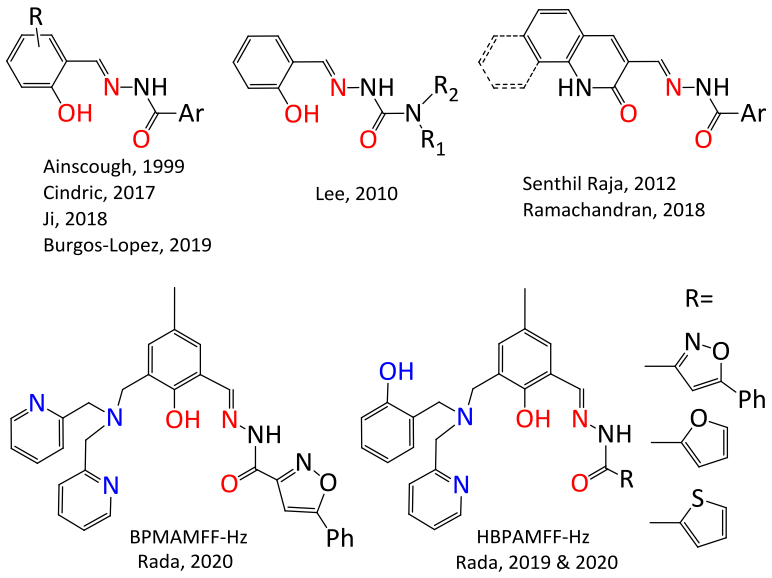

Fig. 1 A few examples of aroylhydrazones used for copper(II) chelation.

On the other hand, due to their excellent photophysical properties, boron dipyrromethene (BODIPY) fluorophores have extensively been employed to track metal complexes within cells[17], including several mononuclear copper complexes[18-21]. Similarly, benzopyranothiophene (BPT) is a well-known fluorophore whose hydrazide derivative was successfully used to stain glycoproteins in gels[22].

In the present paper, we report two new unsymmetrical binucleating ligands based on the HBPAMFF-Hz scaffold, where a BPT or BODIPY fluorescent entity was appended to the aroylhydrazone portion of the molecule (Figure 2): (1) to assess their ability to enter cancer cells and (2) to determine their subcellular localization. The HBPAMFF-derived ligands carrying a fluorescent moiety were synthesized from the aldehyde and respective hydrazide precursors and four dinuclear copper(II) complexes were obtained by reaction with $Cu(ClO_4)_2{\cdot}6H_2O$ or $Cu(OAc)_2{\cdot}H_2O$. The spectroscopic properties of the ligands and complexes were studied in detail, and their cytotoxic activity was investigated on the triple negative human breast cancer cell line MDA-MB-231 through the MTT assay. The BODIPY-containing ligand was finally imaged in cancer cells by fluorescence microscopy, including colocalization studies with organelle stains.

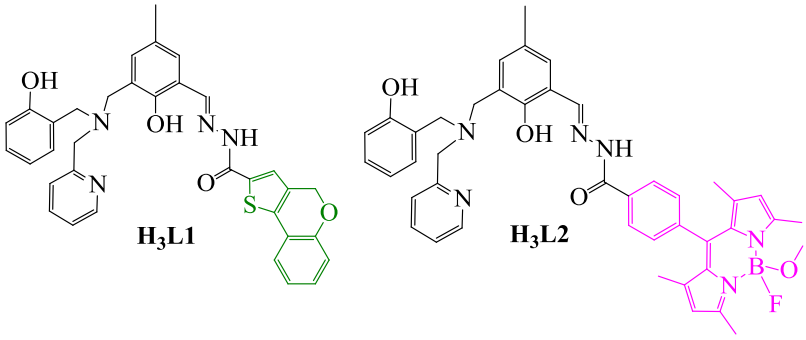

Fig. 2 Chemical structure of ligands **H_3L1** and **H_3L2**.

2. Materials and methods

2.1. Materials

4-methoxycarbonyl benzaldehyde, tetrachloro-1,4-benzoquinone (chloranil) and 2,4-dimethylpyrrole were from TCI Chemicals. Additional reagents for the synthesis of BODIPY precursors were purchased from Acros Organics and/or Sigma-Aldrich. All other chemicals were obtained from Sigma-Aldrich, and were used without further

purification. On the other hand, the precursor 3-[(2-hydroxybenzyl)(2-pyridylmethyl)aminomethyl]-2-hydroxy-5-methylbenzaldehyde was synthesized as previously described[23].

2.2. Instrumentation

Absorption spectra were recorded with Lamba 35 (Perkin-Elmer), Cary 100 (Agilent) or Cary 50 (Varian) spectrophotometers, under controlled temperature. The fluorescence spectra were recorded with a FP-6200 spectrofluorimeter (Jasco). The 1D and 2D NMR spectra were acquired on Bruker Avance III HD-400 or Bruker Avance III nanobay 400 spectrometers. ^{1}H NMR peaks were calibrated using the solvent reference for DMSO-d_6 or $CDCl_3$ at 2.50 and 7.26 ppm, respectively. Coupling constants (J) were quoted in Hz and chemical shifts (δ) in ppm. Infrared spectra in KBr pellets were recorded with a Spectrum 400 FTIR spectrometer (Perkin-Elmer) at 4 cm^{-1} resolution. Mass spectra were recorded with a TQ R30-10 HRMS spectrometer in the positive mode and are given in m/z for positive ions. Complexes were diluted in methanol (> 99.9 %, 990 µL). Samples presented a clear aspect, without suspended particles at final concentration about 10 (± 20%) µg mL^{-1}. Elemental analyses were carried out in triplicate with a Flash EA 1112 analyser (Thermo Electron). Inductively coupled plasma optical emission (ICP-OES) spectra in water were acquired with a Perkin-Elmer Optima 7300 DV spectrometer using a dye laser pulsed copper line at 324.7 nm. Complexes were digested with nitric acid before aqueous dilution. The conductivity of the complex solutions (MeCN; 1×10^{-3} mol L^{-1}; room temperature) was measured by using an electrical conductivity 650MA Analyser. Data processing was carried out in the softwares provided by the manufacturers.

The X-ray intensities data of a single crystal of **1**, were collected at 200 K using graphite-monochromated Mo $K\alpha$ radiation (λ = 0.71073 Å) with a Bruker Kappa APEX-II CCD diffractometer. Unit-cell parameters determination, integration and data reduction were carried out through the SAINT program. SADABS was used for scaling and absorption corrections. The structure was solved with SHELXT[24] and refined by full-matrix least-squares methods with SHELXL[25] using Olex2 software package[26]. All non-hydrogen atoms were refined anisotropically. Symmetry codes and data deviation were obtained by employing the PLATON software. Distances and angles were calculated with DIAMOND or, alternatively, MERCURY softwares. Supplementary crystallographic data for **1** can be found in supporting information (Tables S2-S4) and in the Cambridge Crystallographic Data Centre database (CCDC deposit number 2039356).

2.3. Syntheses of precursors

2.3.1. 4-MePh-BODIPY

Precursor 5,5-difluoro-10-(4-methoxycarbonylphenyl)-1,3,7,9-tetramethyl-BODIPY (4-MePh-BODIPY was synthesized from 4-methoxycarbonylbenzaldehyde (4-MeBA) and 2,4-dimethylpyrrole as previously reported[27], with slight modifications. The light-yellow reaction medium containing 4-methoxycarbonylbenzaldehyde (328 mg, 2

mmol) and 2,4-dimethylpyrrole (380 mg, 4 mmol) was stirred in dry DCM under an argon atmosphere and room temperature for 20 min. Then, one drop of trifluoroacetic acid (TFA) was added to the solution, which immediately turned to dark red and, then, the solution was stirred overnight at room temperature. Subsequently, solid tetrachloro-1,4-benzoquinone (chloranil) (492 mg, 2 mmol) was added and the solution was stirred for 1 h. Then TEA (6 mL) was added, and the solution was stirred for 30 min. After, boron trifluoride diethyl etherate (6 mL) was slowly added to the solution, which was stirred for another 2 h. The fluorescence of the solution was verified under a UV lamp. The solution was washed three times with distilled water (70 mL). Whenever a black solid precipitated, the solution was filtered under reduced pressure through a layer of cotton. The organic phase was dried with anhydrous $MgSO_4$ and the solvent evaporated. The resulting solid (6 g) was purified by column chromatography using SiO_2 (200 g) as the stationary phase and cyclohexane/ethyl acetate 8:1 as eluent. When necessary, the product was purified a second time, under the same conditions. Yield = 105 mg (14%).

2.3.2. FMeO-BODIPY-Hz

5-fluoro-5-methoxy-10-(4-methoxycarbonylphenyl)-1,3,7,9-tetramethyl-BODIPY (FMeO-BODIPY-Hz) was synthesized from 4-MePh-BODIPY (140 mg, 0.37 mmol) and hydrazine hydrate $H_2NNH_2{\cdot}H_2O$ (6 mL), under an inert argon atmosphere, following the procedures previously described[28]. The reaction was monitored by TLC employing cyclohexane/ethyl acetate 8:1 as the eluent. When 4-MePh-BODIPY was completely consumed (after 24 h), MeOH was evaporated under vacuum. The residue was dissolved in 70 mL DCM and washed 3 times with water (70 mL). The aqueous phase was extracted once with DCM (20 mL). Solvent was dried with anhydrous $MgSO_4$ and evaporated after filtration. The resulting solid (100 mg) was purified by column chromatography using SiO_2 (50 g) as the stationary phase and chloroform/MeOH/ammonium hydroxide 100:5:1 as eluent. When necessary, the product was purified a second time in the same conditions. Yield = 79.1 mg (54%). ^{1}H NMR (400 MHz, $CDCl_3$, Figure S2): ∂ in ppm 7.92 (*t*, 2H, *J* = 8 Hz, CH_{Ph}), 7.42 (*t*, 2H, *J* = 8 Hz, CH_{Ph}), 5.98 (*s*, 2H, CH_{BODIPY}), 2.99 (*s*, 3H, OCH_3), 2.55 (*s*, 6H, CH_3) and 1.35 (*s*, 6H, CH_3). ^{13}C NMR (100 MHz, $CDCl_3$): ∂ in ppm 156.3 (Ph, C=O), 142.1 (2xC-Me_{BODIPY}), 140.1 (BODIPY-C_{Ph}), 139.3 (Hz-C_{Ph}), 131.8 (Ph-C_{BODIPY}), 129.0 (2xCH_{Ph}), 128.9 (2xCH_{Ph}), 127.9 (2xC_{BODIPY}), 127.7 (2xC_{BODIPY}), 121.6 (2xCH_{BODIPY}), 49.3 ($OCH_{3BODIPY}$), 29.8 (2x$CH_{3BODIPY}$), and 14.7 (2x$CH_{3BODIPY}$).

2.4. Syntheses of ligands

2.4.1. **H_3L1**

Aldehyde **HBPAMFF** (1.6 mmol, 579.9 mg) and 4*H*-[1]-benzopyrano[4,3-*b*]thiophene-2-carbohydrazide (BPTH) (1.6 mmol, 394.1 mg) were dissolved separately in DMSO/MeOH 3:1 (40 mL). BPTH was slowly added to the **HBPAMFF** solution. The resulting mixture was stirred and heated for 3 h at 65 °C. The yellow precipitate formed

was then filtered, washed with ice-cold MeOH and dried overnight under reduced pressure at 80 °C to remove eventual solvent residues. M.p. = 215 °C, yield = 945 mg (1.6 mmol, 99%). The solid was recrystallized in DMK/MeOH 1:1. Elem. Anal.: calcd. (%) for $C_{34}H_{30}N_4O_4S$ (590.77 g mol^{-1}): C 69.1, H 5.1, N 9.5, S 5.4; found: C 68.4, H 5.1, N 10.3, S 5.5.

2.4.2. **H_3L2**

HBPAMFF (0.08 mmol, 29.0 mg) was dissolved in MeOH (2 mL) and the solution heated for some minutes, and then leaved to cool down to room temperature. FMeO-BODIPY-Hz (0.08 mmol, 31.5 mg) was dissolved separately in MeOH (4 mL) and added dropwise to the **HBPAMFF** solution. The reaction mixture was heated for 2 h at 65 °C and, then, stirred overnight at room temperature. Monitoring the reaction solution by TLC (using as eluent DCM/MeOH/NH_4OH 10:0.5:0.1) showed that the fluorescent precursor FMeO-BODIPY-Hz was consumed. The mixture was then transferred to a beaker and the solvent, removed with a Pasteur pipette. The cinnabar red solid was washed by dropping ice-cold MeOH and removing the solvent with a Pasteur pipette (three times). The product was dried at room temperature. Small crystals were obtained by recrystallizing the product in MeCN. M.p. = 220 °C, yield = 37 mg (0.05 mmol, 63%). Elem. Anal. calcd. (%) for $C_{43}H_{44}N_6O_4BF$ (738.66 g mol^{-1}): C 69.9, H 6.0, N 11.4; found: C 68.3, H 6.1, N 12.5.

2.5. Syntheses of complexes

Caution! *Perchlorate salts of metal complexes containing organic ligands are potentially explosive and should be handled with care and prepared in small amounts.*

2.5.1. Complex **1**

H_3L1 (0.3 mmol, 177.2 mg) was dissolved in THF/MeOH 2:1 (60 mL) under heating for some minutes. The solution was then left to cold down and, when it reached the room temperature, copper(II) perchlorate hexahydrate (0.6 mmol, 222.3 mg) dissolved in 5 mL MeOH was dropwise added to the yellow ligand solution, which suddenly became dark green upon complexation. After 40 min of heating at 65 °C, KOH (1 M, 1.5 mmol, 1.5 mL in MeOH) was added, and stirring was kept for 20 min. The next day, the solvent was removed, and the product was washed by successively dropping and removing ice-cold MeOH with the aim of a Pasteur pipette. Solid was dried in air. When recrystallized by slow evaporation of a DMSO solution, the complex formed dark green single crystals suitable for XRD analysis. Yield = 210.9 mg (0.21 mmol, 70%). Elemental analysis: calcd. (%) for $[Cu_2(C_{34}H_{28}N_4O_4S)(MeOH)(ClO_4)_2(OH_2)]\cdot H_2O\cdot MeOH$ (1014.76 g mol^{-1}): C 42.6, H 4.0, N 5.5; found: C 42.7, H 3.9, N 5.3. ICP-OES calcd.: Cu 14.0; found: 14.2%.

2.5.2. Complex **2**

H_3L1 (0.3 mmol, 177.2 mg) was dissolved in THF/MeOH 2:1 (60 mL). Copper(II) acetate monohydrate (0.66 mmol, 131.8 mg, in 10 mL MeOH) was then dropwise added to the ligand, and the reaction solution was heated for 40 min. The oil obtained was diluted in MeCN (30 mL) and the light green precipitate formed was filtered, washed with ice-cold MeOH and dried under reduced pressure. Yield = 198.9 mg (0.22 mmol, 75%). Elemental analysis: calcd. (%) for $[Cu_2(C_{34}H_{28}N_4O_4S)(O_2CMe)_2(OH_2)]\cdot 2H_2O$ (888.91 g mol^{-1}): C 51.4, H 4.5, N 6.3, S 3.5; found: C 50.7, H 4.4, N 6.9, S 4.2. ICP-OES calcd.: Cu 14.3; found: 14.6%.

2.5.3. Complex **3**

This compound was synthesized from **H_3L2** (0.024 mmol, 17.7 mg) in MeOH (2.5 mL) and copper(II) perchlorate hexahydrate (0.048 mmol, 17.8 mg, in 2.5 mL MeOH), following a procedure very similar to that described for complex **1**. The dark green solid obtained was dried in open atmosphere. Yield = 23.5 mg (0.018 mmol, 73%). Elemental analysis: calcd. (%) for $[Cu_2(C_{43}H_{43}N_6O_4BF)(OH_2)_3](ClO_4)_3\cdot 7H_2O$ (1343.25 g mol^{-1}): C 38.5, H 4.7, N 6.3; found: C 37.5, H 4.4, N 6.1. ICP-OES calcd.: Cu 9.5; found: 9.7%.

2.5.4. Complex **4**

This compound was synthesized from **H_3L2** (0.024 mmol, 17.7 mg) in MeOH (2.5 mL) and copper(II) acetate monohydrate (0.048 mmol, 9.6 mg, in 10 mL MeOH), by following a procedure very similar to that described for complex **2**. The dark red solid was dried in open atmosphere. Yield = 13.4 mg (0.012 mmol, 50%). Elemental analysis: calcd. (%) for $[Cu_2(C_{43}H_{42}N_6O_4BF)(O_2CMe)(OH_2)_2](MeCO_2)\cdot 5H_2O$ (1107.93 g mol^{-1}): C 50.9, H 5.6, N 7.6; found: C 50.3, H 5.5, N 7.1. ICP-OES calcd.: Cu 11.5; found: 11.8%.

2.6. Stability studies

The absorption spectra of the compounds were monitored in DMSO, in PBS/DMSO 9:1 at pH 7.40 and in Dulbecco's Modified Eagle Medium (DMEM) supplemented with 10% fetal bovine serum, Glutamax I and 1% kanamycin during 72 h. The stability was assessed from the absorbance of the most intense band of each ligand or complex.

2.7. Cytotoxicity assays

MDA-MB-231 cells were cultivated in atmosphere containing 5% CO_2 at 37 °C in DMEM supplemented with 10% fetal bovine serum, Glutamax I and 1% kanamycin. The stock solutions of ligands and complexes (1 mM) were prepared in DMSO and sterilized by filtration on 0.20 µm PTFE-20/25 syringe filters. Cells were seeded at 2×10^3 cells/well (100 µL) in 96-well plate. After 24 h, cell medium was aspirated and replaced by solutions of ligands or complexes (0.01 – 10 µM) and fresh cell culture medium with DMSO adjusted to 1% (v/v). Cells were incubated for another 72 h at 37 °C under 5% CO_2.

The growth inhibitory effect of the compounds was determined using the colorimetric 3-(4,5-dimethylthiazol-2-yl)-2,5-diphenyl tetrazolium bromide (MTT) assay. Cells were incubated for 3 h at 37 °C plates containing MTT (0.5 mg mL^{-1} in culture medium, 20 μL/well). After discarding supernatants and addition of DMSO (200 μL), the plates were mixed gently for some minutes in a variable-speed rocker. Absorbance (λ = 560 nm) was recorded with a microplate reader (Fluostar Optima, BMG Labtech) and corrected by subtracting the absorbance background. The percentage of surviving cells was calculated as the ratio of the absorbance of treated to untreated cells. The dose-dependent effect profile was obtained by plotting the cell viability (%) as a function of the concentration (μM) of each compound. Curves were fitted to a sigmoidal logistic function, and the concentration necessary to decrease cell proliferation by 50% (IC_{50}) was obtained by interpolating from the resulting equations. The reported IC_{50} values are presented as the mean of triplicate experiments (mean ± S.D).

2.8. Cellular uptake and localization

The emissive properties of ligand **H_3L2** were used to examine the cellular uptake and localization of the compound in MDA-MB-231 cancer cells by fluorescence microscopy. MDA-MB-231 cells were seeded in a 24-well plate at a density of 1×10^5 cells per well (volume: 500 μL) in DMEM supplemented with 10% fetal bovine serum, Glutamax I and 1% kanamycin. Cells were grown for 24 h under humidified atmosphere containing 5% CO_2 at 37 °C. After this period, cell medium was discarded from the wells, replaced by a solution containing **H_3L2** (1 μM) in culture medium and incubated for 3 h at 37°C. MDA-MB-231 cells were further treated with the mitochondria-staining dye MitoTracker Red™ (MTR, 200 nM) for 45 min. Subsequently, culture medium was discarded and cells were washed twice with PBS (1 mL) and treated with a solution of paraformaldehyde in PBS (4%; 1.5 mL) for 8 min at room temperature. The paraformaldehyde solution was then removed and cells were washed twice with PBS (1 mL). Cells were then treated with the nucleus-staining dye 4′,6-diamidino-2-phenylindole (DAPI, 300 nM).

Images were obtained employing a Delta-Vision imaging system (GE Healthcare), with an Olympus IX71 inverted microscope, a 40x objective (NA 0.8) and Softworx software. Deconvolution was performed using Huygens Deconvolution Software (SVI).

3. Results and discussion

3.1. Syntheses and characterization of the ligands and their dicopper(II) complexes

Reaction of precursor 3-[(2-hydroxybenzyl)(2-pyridylmethyl)aminomethyl]-2-hydroxy-5-methylbenzaldehyde (a.k.a. **HBPAMFF**, in short)[29] with commercially available 4H-[1]-benzopyrano[4,3-b]thiophene-2-carbohydrazide (BPTH) in a mixture of methanol and acetonitrile afforded the aroylhydrazone **H_3L1** in excellent yield (Scheme 1). This ligand crystallized as small colorless hexagonal crystals from the reaction medium. The ^{1}H NMR spectra of **H_3L1** is rather complicated (Figure S3; see assignments in Table S1).

Aroylhydrazones can exist as two stereoisomers at the imine bond (*E* / *Z*) and as two conformations at the amide bond (*anti* / *syn*)[30]. Moreover, two tautomeric forms (amide / iminol) are possible. In DMSO-d_6, the proton of the imine bond (8.62 and 8.45 ppm) and the one of the amide bonds (12.12 and 11.77 ppm) appear as two pairs of singlets in the proportion of 67 to 33%. According to the literature[30], this is typical of an (*E*)-stereoisomer with the amide OC–NH bond alternatively adopting *anti* and *syn* conformations. The (*E*) isomer is most probably favored by the presence of a hydrogen bond between the azomethine nitrogen and the hydroxyl group of the central phenol.

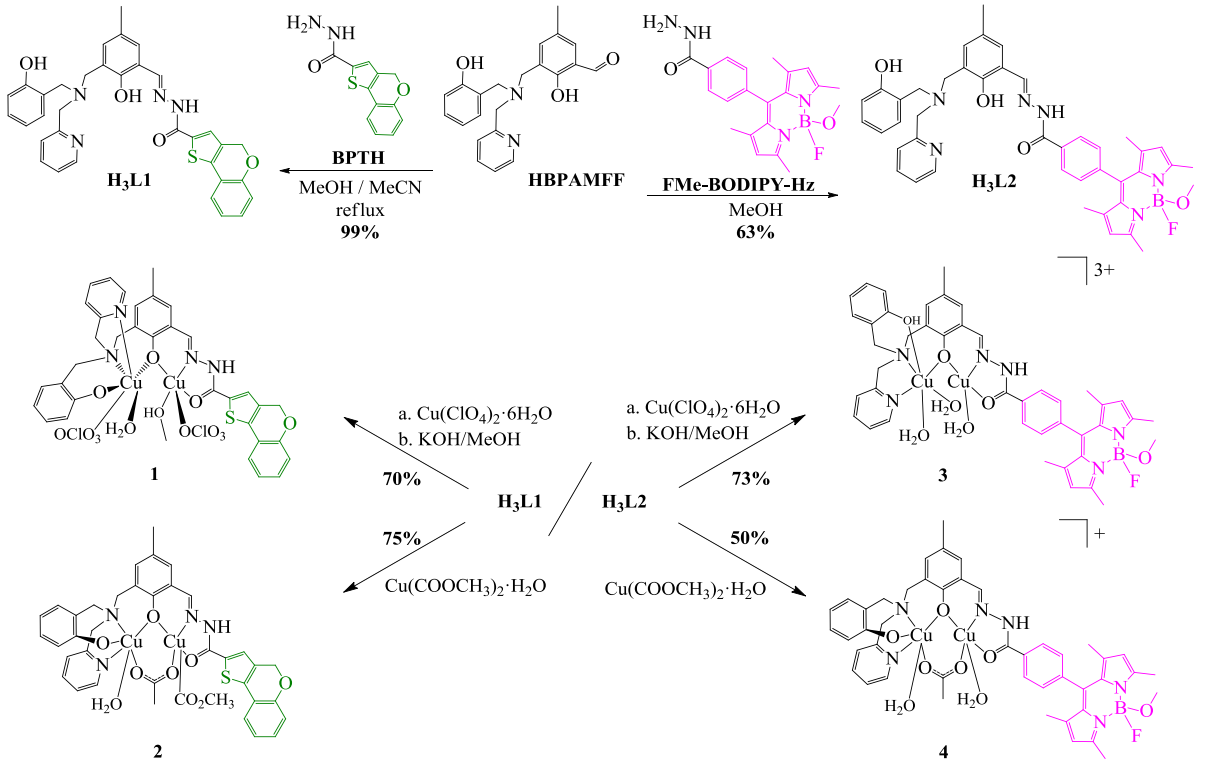

Scheme 1 Synthetic routes to ligands **H_3L1** and **H_3L2** (top), and their dicopper(II) complexes from perchlorate, **1** and **3**, or acetate, **2** and **4**, salts (bottom). In the case of the acetato complexes, the coordination mode of this anion was suggested on the basis of a structure-related compound previously published by our group[16].

To synthesize the BODIPY-carrying hydrazonic ligand **H_3L2**, we first prepared the *N*-acyl-hydrazide precursor by reacting a BODIPY derivative containing the methyl benzoate substituent at the *meso* position[27] with hydrazine hydrate in refluxing MeOH (Scheme S1), following literature protocols[28, 31]. Surprisingly, instead of obtaining the expected difluoro BODIPY hydrazide product, a mixture of three compounds was formed and the main product was identified as the monomethoxy derivative FMeO-BODIPY-Hz, resulting from the substitution of one fluoro substituent at the boron atom. The reaction of this precursor with **HBPAMFF** in MeOH gave the expected hydrazone in satisfactory yield (Scheme 1). Both in the solid state and in solution, **H_3L2** was cinnabar

red (Figure S23). The ^{1}H NMR spectrum of this ligand in DMSO-d_6 (Figure S5, with assignments in Table S1) presents only one set of signals, which is in agreement with the presence of a single stereoisomer-conformation combination [most probably the (*E*)-*anti* form].

The corresponding copper(II) complexes **1**–**4** were prepared in good yields from **H_3L1** or **H_3L2** and 2 eq. copper perchlorate in the presence of KOH, to afford compounds **1** and **2**, or directly with copper acetate, to obtain **3** and **4**. Complexes **1** and **3** were dark green, while **2** and **4** were, respectively, light green and dark red (see Figure S23 for the BODIPY-containing compounds **3** and **4**). The electrolyte nature of the complexes was analyzed by conductivity measurements. The insignificant molar conductivity of **1** (34 $\Omega^{-1}\cdot cm^2\cdot mol^{-1}$) and **2** (7 $\Omega^{-1}\cdot cm^2\cdot mol^{-1}$) in acetonitrile indicated that they are non-electrolyte systems, whereas complexes **3** (362 $\Omega^{-1}\cdot cm^2\cdot mol^{-1}$) and **4** (134 $\Omega^{-1}\cdot cm^2\cdot mol^{-1}$) belong to the 1:3 and 1:1 electrolyte groups, respectively[32]. Combined with the elemental analysis data, these results allowed to formulate the complexes derived from the BPT-containing ligand **H_3L1** as $[Cu_2(\mathbf{HL1})(MeOH)(ClO_4)_2(OH_2)]\cdot H_2O\cdot MeOH$ (**1**) and $[Cu_2(\mathbf{HL1})(O_2CMe)_2(OH_2)]\cdot 2H_2O$ (**2**). Similarly, complexes derived from the BODIPY-related ligand **H_3L2** can be formulated as $[Cu_2(\mathbf{H_2L2})(OH_2)_3](ClO_4)_3\cdot 7H_2O$ (**3**) and $[Cu_2(\mathbf{HL2})(O_2CMe)(OH_2)_2](MeCO_2)\cdot 5H_2O$ (**4**). In complex **3**, we propose that the terminal phenol group from **H_3L2** remains protonated after coordination, as reported by us for similar systems[16].

3.2. Crystal structure

The molecular structure of **1** was determined by X-ray diffraction analysis of a single crystal. Complex **1** crystallized in the triclinic system, space group P-1. Figure 3 shows a view of the structure. In addition to a doubly deprotonated **$HL1^{2-}$** unit, two perchlorate ions from the metal salt, as well as one water and one methanol molecules act as ligands for the copper(II) centers. One free water and one free methanol molecules complete the asymmetric unit. Table 1 gathers selected bond distances and angles. The crystallographic data and refinement parameters (Table S2), along with a comprehensive list of bond distances/angles for **1** (Table S3) can be found as supplementary information.

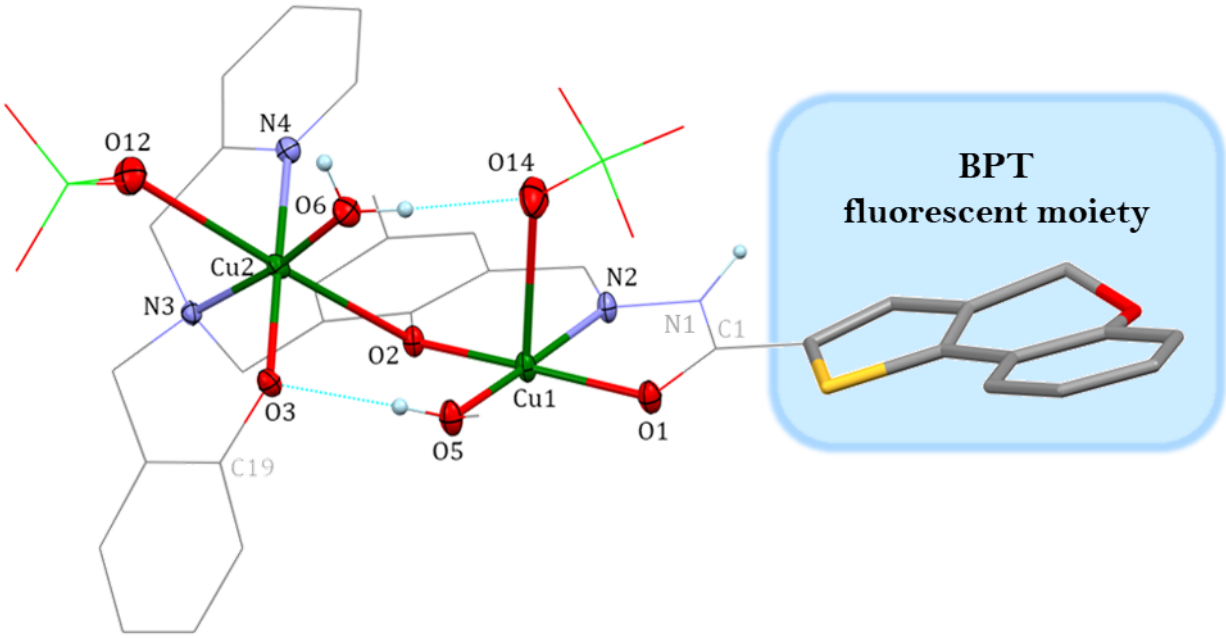

Fig. 3 Crystal structure representation of a molecule of **1**. Copper coordination environment is highlighted, as well as the BPT fragment. Most of the hydrogen atoms, the free crystallization solvents and the minor position of a disordered perchlorate ion are omitted for the sake of clarity. Only hydrogen atoms involved in hydrogen bonds are shown. Intramolecular H-bonds are depicted as light blue dotted lines. All non-hydrogen atoms were refined anisotropically.

Table 1 Selected geometric parameters for complex **1**

Bond lengths (Å)		Bond angles (°)			
Cu1–O1	1.9743(14)	O1–Cu1–O2	173.70(6)	O3–Cu2–N3	94.55(6)
Cu1–O2	1.8879(13)	N2–Cu1–O5	173.29(7)	O3–Cu2–O6	86.03(6)
Cu1–O5	1.9396(15)	O1–Cu1–N2	81.65(6)	N4–Cu2–N3	84.03(6)
Cu1–N2	1.9205(16)	O1–Cu1–O5	94.45(6)	N4–Cu2–O6	95.64(7)
Cu1–O14	2.6020(22)	O2–Cu1–N2	93.62(6)	O3–Cu2–O2	85.254(54)
Cu2–O2	2.4795(13)	O2–Cu1–O5	90.65(6)	N3–Cu2–O2	88.566(57)
Cu2–O3	1.9433(14)	O1–Cu1–O14	89.111(63)	N4–Cu2–O2	90.938(63)
Cu2–O6	1.9801(15)	N2–Cu1–O14	81.696(71)	O6–Cu2–O2	99.816(58)
Cu2–N3	2.0072(16)	O2–Cu1–O14	94.346(59)	O12–Cu2–O3	97.921(61)
Cu2–N4	1.9889(16)	O5–Cu1–O14	92.828(70)	O12–Cu2–N3	88.327(63)
Cu2–O12	2.6482(18)	O2–Cu2–O12	174.160(56)	O12–Cu2–N4	83.821(67)
		O3–Cu2–N4	177.73(6)	O12–Cu2–O6	83.312(63)
		N3–Cu2–O6	171.62(6)		

Crystallographic data indicate that, in this crystal phase, the precursor hydrazonic ligand is deprotonated at both phenol sites but conserves the –HN–CO– hydrogen atom, which clearly characterizes its coordination as occurring in the amido tautomeric form. This is also substantiated by the presence of a H-bond between the amide hydrogen and a water molecule (see below). The C1–O1 distance [1.265(2) Å] typically corresponds to a double bond. For the sake of comparison, C19–O3 distance in the terminal phenoxo group is much larger, displaying a value of 1.353(2) Å.

The complex exhibits two independent copper sites with a 3.757 Å inter-metallic distance. Cu1 ion is pentacoordinated in an almost perfect square pyramidal geometry ($\tau \cong 0.01$). Equatorial plane comprises the **HL1**$^{2-}$-derived hydrazonic N2 and O1 atoms and, acting as a dissymmetric bridge between both copper centers, the phenoxo O2 donor. The pyramidal base is completed by a methanol molecule (O5 atom). Copper-donor atom distances in this plane range between 1.888(1) Å and 1.974(1) Å. The apical position is occupied by the O14 atom from a perchlorate anion, located at a much larger distance. On the other hand, Cu2 is hexacoordinated. Four of these coordination sites are filled by the **HL1**$^{2-}$ ligand: besides the axial position occupied by the bridging phenoxo group (O2), three out of four equatorial sites involve coordination to N3, N4 and O3 atoms from the **HBPAMFF** moiety of **HL1**$^{2-}$. A water molecule (O6 atom) completes this N_2O_2-plane, which displays Cu2–donor bond distances varying from 1.943(1) to 2.007(2) Å. Finally, the O12 atom, which belongs to a second perchlorate anion, interacts axially with Cu2 completing the coordination sphere. As it can be easily noticed, the Cu2 center presents a pronounced Jahn-Teller elongation. Two intramolecular H-bonds involving coordinated solvent molecules are observed in the structure: O5(methanol)–H5···O3(terminal phenolate group) and O6(water)–H6B···O14(perchlorate coordinated to Cu1).

In the crystal packing (Figure S7A), the molecules of **1** are pairwise arranged, with two units of the complex interacting through intermolecular H-bonds through crystallization, structural methanol molecules (atoms designated by *): O6–H6A···O7* [2.6275(25) Å] and O7*–H7*···O10^{i}(perchlorate bound to Cu2^{i}) [3.0443(36) Å] [*Symmetry code (i): 2 − x, 1 − y, 1 − z*]. A one-dimensional network of these dimers along the crystallographic axis *a* (Figure S7B) is generated by another set of intermolecular H-bond interactions which involve crystallization, structural water molecules (atoms denoted by †); namely, O8†–H8A†···O3^{ii} [2.7339(18) Å], O8†–H8B†···O9^{ii}(perchlorate bound to Cu2^{ii}) [2.8771(26) Å] [*Symmetry code (ii): − 1 + x, y, z*], and N1–H1···O8† [2.7138(30) Å]. The O7*–H7*···O9 last intermolecular H-bond and weak van der Waals interactions also contribute to the crystal cohesion. A complete panorama of the H-bond geometries present is available in Table S4.

3.3. Mass spectrometry

As single crystals suitable for structure determination were not obtained for **2**, **3** and **4**, electrospray ionization high-resolution mass spectra (ESI-HRMS) were recorded in the

positive mode to get insight into the nature of the species present in solutions of these complexes (Figures S8 – S10). For the acetate-containing compounds **2** and **4**, the molecular ion peaks at m/z 745 and 893 can be assigned to the $[Cu_2(HL)(OCH_3)]^+$ species resulting from the loss of aquo and acetato ligands and the coordination of a deprotonated H_3CO^- group derived from methanol used as a solvent in the analyses. On the other hand, the mass spectrum of compound **3** was more complex, with peaks at m/z 881, 833 and 418. The first one is associated to $[Cu_2(\mathbf{H_2L2})(OH_2)]^+$, as deduced from the comparison with its simulated high-resolution mass spectrum (Figure S9B). The monovalent (z=+1) nature of this species can only be explained by the concomitant reduction of both copper(II) centers to copper(I)[33]. Finally, the peak at m/z 418 is probably related to a doubly charged complex. All mono-cationic species proposed are in complete agreement with the calculated isotopic distribution pattern (Figures S8B – S10B). It is worth noting that no m/z peaks related to the free ligands were observed in any of the spectra.

3.4. *IR spectroscopy*

The FTIR spectra (solid state, KBr) of the ligands show bands at around 3200 cm^{-1} ($\nu_{N\text{-}H}$), 1665 cm^{-1} ($\nu_{C=O}$; Amide I band), 1550 cm^{-1} ($\partial_{N\text{-}H}$ + $\nu_{C\text{-}N}$; Amide II band) and at 1620 cm^{-1} ($\nu_{C=N}$), related to the *N*-acyl-hydrazone moiety. The displacement of the C=O stretching frequency upon complexation, whose bands appear overlapped to those of $\nu_{C=N}$, confirms the involvement of this group in the interaction with copper(II). Moreover, the presence of the N–H stretching/bending absorptions in the spectra of all complexes indicates that coordination occurs in the amido form for both ligands, as confirmed, in the case of compound **1**, through the X-ray diffraction analysis. Additionally, the spectra of complexes **1** and **3** displayed strong characteristic vibration bands due to perchlorate modes at 1085/1087 (ν_3), 954/955 (ν_4), and 626/627 cm^{-1}[34]. The most relevant absorptions, along with the proposed assignments, are displayed in Table S5 and Figures S11–S16.

3.5. Photophysical properties

Electronic absorption spectra of ligands $\mathbf{H_3L1}$ and $\mathbf{H_3L2}$, their precursors and complexes **1**–**4** in H_2O/DMSO 9:1 are shown in Figures 4A and 4B, respectively. A summary of the absorption properties of $\mathbf{H_3L1}$, $\mathbf{H_3L2}$ and their dicopper(II) complexes **1**–**4**, including the suggested attributions, can be found in Table S6 (supplementary information).

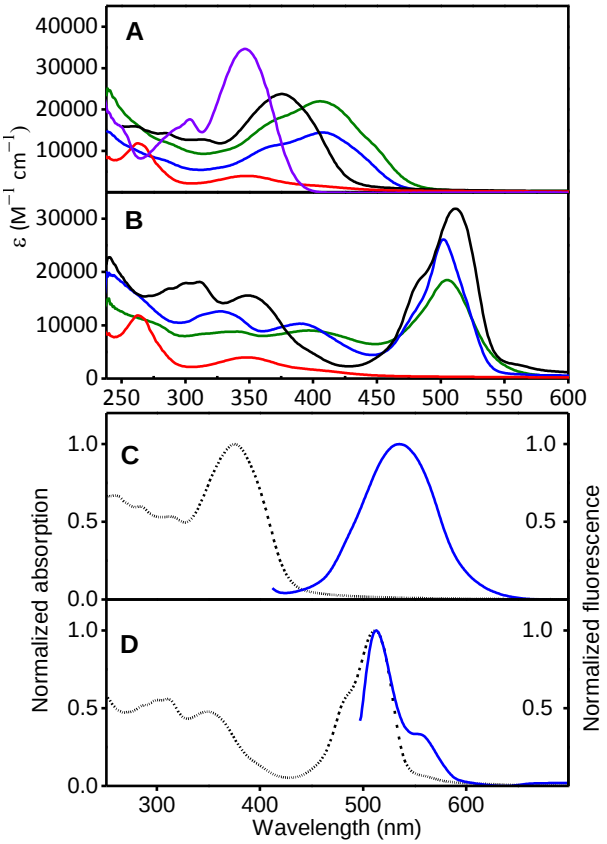

Fig. 4 Absorption spectra of (A) **H_3L1** (black), its precursors **HBPAMFF** (red) and BPTH (purple), and complexes **1** (green) and **2** (blue); and of (B) **H_3L2** (black), its precursor **HBPAMFF** (red), and complexes **3** (green) and **4** (blue) in H_2O/DMSO 9:1 at room temperature. Superimposition of absorption (dotted black line) and fluorescence (blue line) spectra of ligands (C) **H_3L1** (λ_{ex} = 376 nm; 6 μM) and (D) **H_3L2** (λ_{ex} = 485 nm; 50 nM) in H_2O/DMSO 9:1 at room temperature.

The absorption spectrum of ligand **H_3L1** displays four main bands in the 250–450 nm region. The most intense band is centred at 376 nm and was tentatively assigned to the presence of both **HBPAMFF** and BPT moieties in the structure of the ligand by comparison to the spectra of the precursors. Hence, this band would correspond to π–π* transitions of the aromatic rings. This band underwent a redshift with respect to those related to BPTH and **HBPAMFF**. Electronic transitions associated with the aroylhydrazonic function were assigned to the band centred at 314 nm. In the HBPAMFF-Hz ligands previously reported by our research group, two hydrazonic bands, very close to each other in energy, can be observed in the 290 – 320 nm range[15, 16].

On the other hand, the spectrum of **H_3L2** shows six main absorption bands. The intense band at 511 nm and its shoulder at 483 nm are typical of BODIPY derivatives[35]. Because the BODIPY scaffold does not show any absorption in the 250 – 400 nm range[35], the bands at 286 and 350 nm were assigned to **HBPAMFF** transitions. The remaining absorptions at 300 and 311 nm were attributed to hydrazonic-related transitions.

Overall, the dinuclear copper complexes synthesized from **H_3L1** and **H_3L2** showed close absorption profiles to those of their respective ligands. Nevertheless, complexation of copper by **H_3L1** caused a blue shift of the main ligand band from 376 nm to the shoulders at around 365 or 366 nm, with a simultaneous hypochromic effect. In the spectra of **1** and **2**, a ligand-to-metal charge transfer (LMCT) transition from the terminal phenolate to one of the copper(II) centers was observed at 406 and 408 nm, respectively. Complexation of copper by **H_3L2** caused a red shift of the electronic transitions related to the **HBPAMFF** moiety and the hydrazonic system, while the main bands associated to the fluorescent BODIPY motif in **3** and **4** were slightly blue-shifted, in a similar manner to that described for the BPT fluorophore in **1** and **2**, accompanied by a hypochromic effect.

In addition to the emission properties of the **HBPAMFF** precursor, each ligand includes a non-coordinating fluorescent entity. Therefore, the fluorescence properties of the ligands and their copper(II) complexes were examined in various media. In the tested conditions, **HBPAMFF** presented a weak emission at 511 nm, while the precursor BPTH displayed a strong emission at 456 nm (Figure 5A). Upon excitation at 376 nm, the fluorescence spectrum of **H_3L1** showed an emission band at 536 nm (Figure 5A), corresponding to a Stokes shift of 160 nm. Even though BPTH displays a higher emission than **HBPAMFF**, the fluorescence pattern of **H_3L1** seems to be dominated by that of **HBPAMFF**. The emission intensity of **H_3L1** was highly dependent on the solvent, being maximal in DCM and almost inexistent in acetone, methanol and acetonitrile (Figure 5B). In contrast, both dicopper complexes derived from **H_3L1** do not fluoresce (Figure 5A, *Inset*), the presence of the metal ions being most likely responsible for fluorescence quenching.

Upon excitation at 485 nm, the fluorescence spectrum of **H_3L2** showed an emission band at 513 nm (Figure 6A), corresponding to a very small Stokes shift of only 2 nm, typical of green-emitting BODIPY derivatives[36]. As expected, the ligand displayed a much higher fluorescence intensity in organic solvents (Figure 6B). BODIPY derivatives commonly present a strong emission in organic solvents, while in aqueous solutions emission often dramatically decreases. This effect is related to the formation of dimers or higher non-emissive aggregates in water[37]. Among the copper complexes derived from **H_3L2**, **4** was more fluorescent than **2** in aqueous medium (Figure 6A).

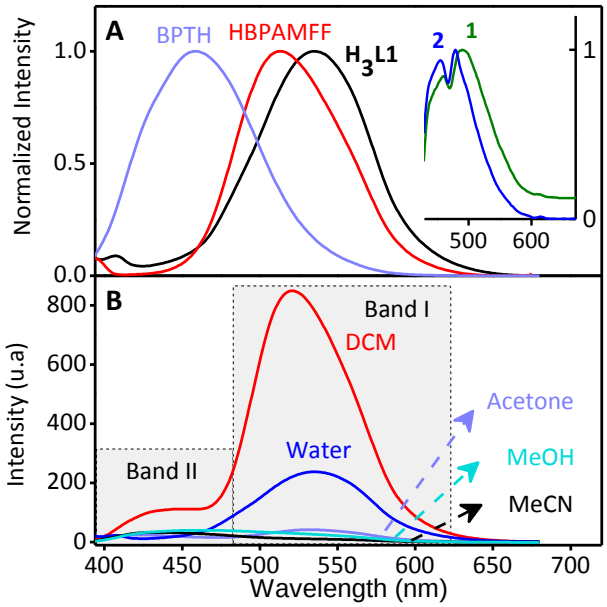

Fig. 5 (A) Normalized fluorescence spectra of ligand **H_3L1** (λ_{ex} = 376 nm; 6 μM), its precursors **HBPAMFF** (λ_{ex} = 349 nm; 40 μM) and BPTH (λ_{ex} = 351 nm; 5 μM) in water at 25 °C. *Inset*: normalized fluorescence spectra of the dicopper complexes **1** (λ_{ex} = 407 nm; 7 μM) and **2** (λ_{ex} = 406 nm; 7 μM). (B) Fluorescence spectra of **H_3L1** (λ_{ex} = 376 nm; 6 μM) in different solvents at 25 °C.

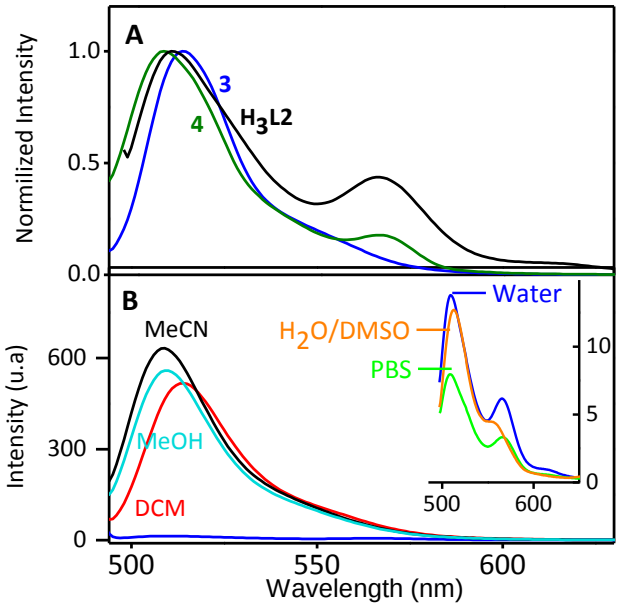

Fig. 6 (A) Normalized fluorescence spectra of ligand **H_3L2** (λ_{ex} = 475 nm; 50 nM), and its complexes **3** (λ_{ex} = 485 nm; 0.3 μM) and **4** (λ_{ex} = 485 nm; 1 μM) in water. (B) The fluorescence spectra of **H_3L2** (λ_{ex} = 475 nm; 50 nM) in different organic solvents. *Inset*: fluorescence spectra of this ligand in water, H_2O/DMSO 9:1 and PBS buffer. Temperature: 25 °C.

3.6. Stability studies

The stability of the potential drugs in biological conditions was evaluated through electronic absorption spectroscopy. For this purpose, the spectra of all compounds were measured in DMSO, PBS and DMEM cell culture medium at 0, 24, 48 and 72 h. In DMSO, and after 72 h, no significant variations were found for **H_3L1**, **H_3L2** and their complexes **1**–**4** (~99% of absorption intensity preserved) indicating good stability for those compounds (Figure S17). It has been reported that, under acidic aqueous conditions, hydrazones could be hydrolyzed. After 72 h in PBS buffer (pH 7.40), the absorption of ligands **H_3L1** and **H_3L2** decreased moderately by 18 % and 17%, respectively, while that of complexes **1**, **2**, **3** and **4** declined by 8%, 42%, 40% and 25% (Figure S18). Nevertheless, the unchanged spectra shapes do not suggest hydrazones' hydrolysis. The spectra absorption decrease could the result of slight compound precipitations. Finally, in DMEM, after the first 24 h, the absorption of the compounds decreased by ~4% (Figure S19) and after 72 h by ~12% (ligands) and by ~4% (complexes), confirming their remarkable stability. With time, the absorption profile of the compounds showed isosbestic points and increase of absorbance of the band centred at ~505 nm. In general, these findings confirmed the adequate stability of the compounds for biological applications.

3.7. In vitro cytotoxicity studies

The *in vitro* antiproliferative activity of ligands **H_3L1** and **H_3L2** and complexes **1**–**4** on the triple negative breast cancer cell line MDA-MB-231 was evaluated by the MTT assay. Cells exposed to the compounds for a period of 72 h at different concentrations had a decrease in their viability as compared to untreated cells (Figure 7). The cytotoxicity profiles of the compounds and the fitted curves for the determination of the IC_{50} values are shown in Figure S20. The ligands, both containing the **HBPAMFF** coordinating moiety, were highly cytotoxic to MDA-MB-231 cells (Table 2), with **H_3L1** having the highest antiproliferative activity of the series (IC_{50} = 90 ± 10 nM). Although the fluorescent fragment attached to the carbonyl side of the hydrazone bond is not involved in metal ion coordination, it has a significant influence on the cytotoxicity towards MDA-MB-231 cells, and the following rank can be established among the various substituents: BPT > BODIPY ~ phenylisoxazole > furane > thiophene (Figure S21)[15, 16]. This result drastically contrasts with some previous reports that showed that aroylhydrazones were inactive[9, 11].

The four copper complexes were also cytotoxic to the MDA-MB-231 cell line, although to a slightly lower extent compared to the corresponding ligands. The perchlorate-derived complexes are somewhat more potent than the respective acetate ones. This difference might be due to the lower biocompatibility of perchlorate with respect to acetate.

This remarkable antiproliferative activity was previously attributed to the capacity of this new family of ligands to sequester intracellular Cu(II) and Fe(III) ions, whereas the

copper complexes can undergo transchelation with Fe(III), creating a depletion of this metal[17]. Alternatively, the complexes could favor the shuttling of copper inside cells, creating a redox imbalance and eventually causing cell death[12].

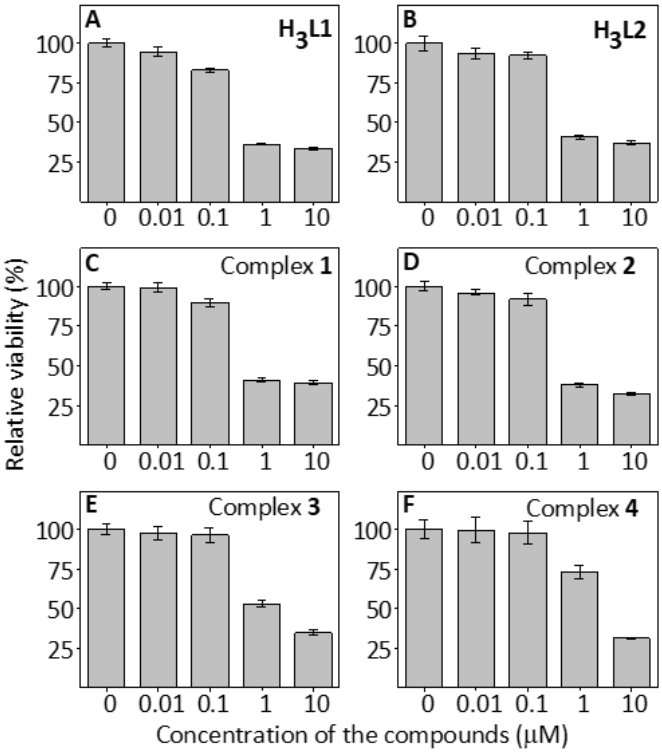

Fig. 7 Dose-dependent effect, expressed as the percentage of relative viability of MDA-MB-231 cells measured by the MTT assay, for ligands (A) **H_3L1** and (B) **H_3L2**, as well as for their dicopper(II) complexes (C) **1**, (D) **2**, (E) **3**, and (F) **4** after 72 h of incubation at 37 °C. Data represent the mean of triplicate experiments.

Table 2 IC_{50} of ligands **H_3L1** and **H_3L2** and their dicopper(II) complexes **1**–**4** on MDA-MB-231 cells. Assays in triplicate (mean ± S.D). Incubation time: 72 h

compound	IC_{50} (μM)	Hz-substituent	counterion
H_3L1	0.09 ± 0.01	BPT	–
H_3L2	0.28 ± 0.02	FMeO-BODIPY	–
1	0.41 ± 0.01	BPT	ClO_4^-
2	0.51 ± 0.08	BPT	CH_3COO^-
3	1.15 ± 0.08	FMeO-BODIPY	ClO_4^-
4	2.71 ± 0.06	FMeO-BODIPY	CH_3COO^-

*3.8. Cellular uptake and localization of **H_3L2** by fluorescence microscopy*

Cellular uptake studies in MDA-MB-231 cells were performed by fluorescence microscopy taking advantage of the luminescence properties of the ligands. **H_3L2** was selected for this study due to its higher emission with respect to **H_3L1**. Live MDA-MB-

231 cells were exposed to **H_3L2** for 3 h at 37 °C. Additionally, cells were treated with the red-emitting mitochondria selective dye MTR, then fixed and further treated with the blue-emitting nucleus selective dye DAPI (Figure 8A). At low concentration (1 μM), ligand **H_3L2** was observed in the cells as visualized by its green-emitting properties, with preferential localization in the perinuclear region (Figure 8B), demonstrating that cellular uptake has occurred. The subcellular distribution of ligand **H_3L2** was close to that of MTR at the resolution of 500 nm (Figure 8C). The comparative distribution of **H_3L2** and MTR was graphically represented by a scatterplot (Figure 8E) where the intensity of the green color was plotted against the intensity of the red color for each pixel of an image comprising a collection of cells (Figure 8D). Colocalization analysis by means of the Fiji software gave a Pearson's correlation coefficient (PCC) of 0.84. This confirms localization of **H_3L2** close to the mitochondria of MDA-MB-231 cells, which is reminiscent of previously published data concerning the mitochondria localization of BODIPY-copper(II) complexes[18, 20].

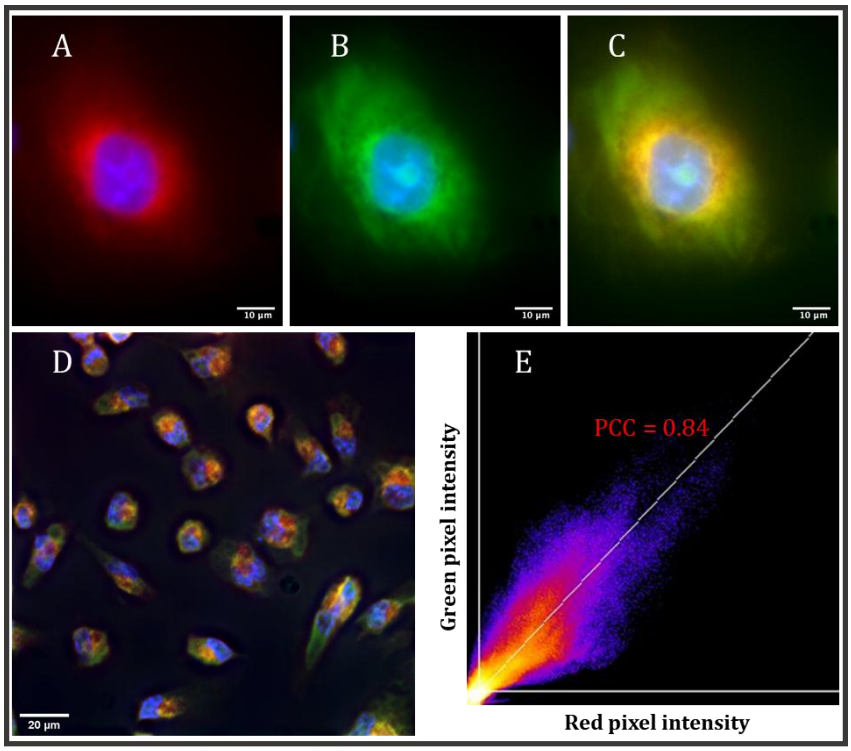

Fig. 8 Fluorescence images of cellular uptake and intracellular localization of ligand **H_3L2** in MDA-MB-231 cells after incubation for 3 h at 37 °C with: (A) DAPI (300 nM) and MTR (200 nM); (B) DAPI and **H_3L2** (1 μM); (C,D) overlay; (E) scatterplot of red and green pixel intensities of cells shown in D. DAPI was excited at 390 nm and emission was recorded at 435 ± 24 nm. MTR was excited at 542 nm and emission was recorded at 597 ± 22 nm. **H_3L2** was excited at 475 nm and emission recorded at 525 ± 18 nm. D size: 164x164 μm.

4. Conclusions

Two novel binucleating hydrazonic ligands containing the fluorescent fragments BPT or BODIPY, as well as their perchlorate dicopper(II) complexes **1** and **3**, and their acetate dicopper(II) complexes **2** and **4** were synthesized and characterized using a large range of analytical techniques. The molecular structure of **1** was confirmed by X-ray diffraction analysis, and its formation involves the partial deprotonation of **H_3L1** and coordination to two copper centers, which display tetragonally distorted octahedral and square pyramidal environments. The absorption and fluorescence profiles of all the compounds obtained were discussed in light of those regarding their respective building blocks.

The cytotoxicity of the compounds was studied by the MTT assay on MDA-MB-231 breast cancer cells, a cell line known to be resistant to usual chemotherapy. The binucleating ligands displayed the highest cytotoxic activity, followed by **1**, the BPT-derived complex containing coordinated perchlorate ions, and by the copper(II) complex with acetate in its structure **2**, which was also prepared from **H_3L1**. The results were compared to those obtained for previously reported HBPAMFF-Hz compounds. The emission properties of ligand **H_3L2**, due to the presence of the FMeO-BODIPY entity, were employed for cellular imaging experiments. They highlighted the ability of this ligand to permeate the MDA-MB-231 cell membrane in a short time and its preferential accumulation in the mitochondria. Interestingly, this work reaffirms that all the **HBPAMFF**-hydrazonic ligands and their copper(II) complexes synthesized up to now present very high antiproliferative activities on cancer cells and may be suitable for future studies as potential anti-tumor agents.

Declaration of competing interest

The authors declare that they have no known competing financial interests or personal relationships that could have appeared to influence the work reported in this paper.

Acknowledgements

Nicolás A. Rey thanks FAPERJ (Fundação Carlos Chagas Filho de Amparo à Pesquisa do Estado do Rio de Janeiro, Brazil) and CNPq (Conselho Nacional de Desenvolvimento Científico e Tecnológico, Brazil) for the research fellowships awarded. J. P. Rada thanks CAPES (Coordenação de Aperfeiçoamento de Pessoal de Nível Superior, Brazil) for the fellowship PDSE-88881.187965/2018-0 and the scholarship 88887.151652/2017-00, as well as CNPq (GM/GD-140228/2018-7). In addition, Prof. Ricardo Q. Aucélio (Department of Chemistry, PUC-Rio) is gratefully acknowledged for the elemental analyses.

Appendix A. Supplementary data

Supplementary data to this article can be found online.

References

[1] R.A. Festa, D.J. Thiele, Copper: an essential metal in biology, Curr. Biol., 21 (2011) R877-883. https://doi.org/10.1016/j.cub.2011.09.040

[2] E.I. Solomon, D.E. Heppner, E.M. Johnston, J.W. Ginsbach, J. Cirera, M. Qayyum, M.T. Kieber-Emmons, C.H. Kjaergaard, R.G. Hadt, L. Tian, Copper Active Sites in Biology, Chem. Rev., 114 (2014) 3659-3853. https://doi.org/10.1021/cr400327t

[3] A. Erxleben, Interactions of copper complexes with nucleic acids, Coord. Chem. Rev., 360 (2018) 92-121. https://doi.org/10.1016/j.ccr.2018.01.008

[4] T.J.P. McGivern, S. Afsharpour, C.J. Marmion, Copper complexes as artificial DNA metallonucleases: From Sigman's reagent to next generation anti-cancer agent?, Inorg. Chim. Acta, 472 (2018) 12-39. https://doi.org/10.1016/j.ica.2017.08.043

[5] C. Santini, M. Pellei, V. Gandin, M. Porchia, F. Tisato, C. Marzano, Advances in Copper Complexes as Anticancer Agents, Chem. Rev., 114 (2014) 815-862. https://doi.org/10.1021/cr400135x

[6] E.W. Ainscough, A.M. Brodie, W.A. Denny, G.J. Finlay, S.A. Gothe, J.D. Ranford, Cytotoxicity of salicylaldehyde benzoylhydrazone analogs and their transition metal complexes: quantitative structure-activity relationships, J. Inorg. Biochem., 77 (1999) 125-133. https://doi.org/10.1016/s0162-0134(99)00131-2

[7] W.Y. Lee, P.P. Lee, Y.K. Yan, M. Lau, Cytotoxic copper(II) salicylaldehyde semicarbazone complexes: mode of action and proteomic analysis, Metallomics, 2 (2010) 694-705. https://doi.org/10.1039/c0mt00016g

[8] D. Senthil Raja, N.S.P. Bhuvanesh, K. Natarajan, DNA binding, protein interaction, radical scavenging and cytotoxic activity of 2-oxo-1,2-dihydroquinoline-3-carbaldehyde(2'-hydroxybenzoyl)hydrazone and its Cu(II) complexes: A structure activity relationship study, Inorg. Chim. Acta, 385 (2012) 81-93. https://doi.org/10.1016/j.ica.2011.12.038

[9] M. Cindrić, A. Bjelopetrović, G. Pavlović, V. Damjanović, J. Lovrić, D. Matković-Čalogović, V. Vrdoljak, Copper(ii) complexes with benzhydrazone-related ligands: synthesis, structural studies and cytotoxicity assay, New J. Chem., 41 (2017) 2425-2435. https://doi.org/10.1039/C6NJ03827A

[10] E. Ramachandran, V. Gandin, R. Bertani, P. Sgarbossa, K. Natarajan, N.S.P. Bhuvanesh, A. Venzo, A. Zoleo, A. Glisenti, A. Dolmella, A. Albinati, C. Marzano, Synthesis, characterization and cytotoxic activity of novel copper(II) complexes with aroylhydrazone derivatives of 2-Oxo-1,2-dihydrobenzo[h]quinoline-3-carbaldehyde, J. Inorg. Biochem., 182 (2018) 18-28. https://doi.org/10.1016/j.jinorgbio.2018.01.016

[11] Y. Burgos-Lopez, J. Del Plá, L.M. Balsa, I.E. León, G.A. Echeverría, O.E. Piro, J. García-Tojal, R. Pis-Diez, A.C. González-Baró, B.S. Parajón-Costa, Synthesis, crystal structure and cytotoxicity assays of a copper(II) nitrate complex with a tridentate ONO acylhydrazone ligand. Spectroscopic and

theoretical studies of the complex and its ligand, Inorg. Chim. Acta, 487 (2019) 31-40. https://doi.org/10.1016/j.ica.2018.11.039

[12] Y. Ji, F. Dai, B. Zhou, Designing salicylaldehyde isonicotinoyl hydrazones as Cu(II) ionophores with tunable chelation and release of copper for hitting redox Achilles heel of cancer cells, Free Radical Biol. Med., 129 (2018) 215-226. https://doi.org/10.1016/j.freeradbiomed.2018.09.017

[13] N.A. Rey, A. Neves, A.J. Bortoluzzi, W. Haase, Z. Tomkowicz, Doubly phenoxo–hydroxo-bridged dicopper(ii) complexes: individual contributions of the bridges to antiferromagnetic coupling based on two related biomimetic models for catechol oxidases, Dalton Trans., 41 (2012) 7196-7200. https://doi.org/10.1039/C2DT30419H

[14] N.A. Rey, A. Neves, A.J. Bortoluzzi, C.T. Pich, H. Terenzi, Catalytic Promiscuity in Biomimetic Systems: Catecholase-like Activity, Phosphatase-like Activity, and Hydrolytic DNA Cleavage Promoted by a New Dicopper(II) Hydroxo-Bridged Complex, Inorg. Chem., 46 (2007) 348-350. https://doi.org/10.1021/ic0613107

[15] J.P. Rada, B.S.M. Bastos, L. Anselmino, C.H.J. Franco, M. Lanznaster, R. Diniz, C.O. Fernández, M. Menacho-Márquez, A.M. Percebom, N.A. Rey, Binucleating Hydrazonic Ligands and Their μ-Hydroxodicopper(II) Complexes as Promising Structural Motifs for Enhanced Antitumor Activity, Inorg. Chem., 58 (2019) 8800-8819. https://doi.org/10.1021/acs.inorgchem.9b01195

[16] J.P. Rada, J. Forté, G. Gontard, V. Corcé, M. Salmain, N.A. Rey, Isoxazole-Derived Aroylhydrazones and Their Dinuclear Copper(II) Complexes Show Antiproliferative Activity on Breast Cancer Cells with a Potentially Alternative Mechanism Of Action, Chembiochem, 21 (2020) 2474-2486. https://doi.org/10.1002/cbic.202000122

[17] B. Bertrand, K. Passador, C. Goze, F. Denat, E. Bodio, M. Salmain, Metal-based BODIPY derivatives as multimodal tools for life sciences, Coord. Chem. Rev., 358 (2018) 108-124. https://doi.org/10.1016/j.ccr.2017.12.007

[18] A. Bhattacharyya, A. Jameei, A. Garai, R. Saha, A.A. Karande, A.R. Chakravarty, Mitochondria-localizing BODIPY–copper(ii) conjugates for cellular imaging and photo-activated cytotoxicity forming singlet oxygen, Dalton Trans., 47 (2018) 5019-5030. https://doi.org/10.1039/C8DT00255J

[19] A. Bhattacharyya, A. Dixit, K. Mitra, S. Banerjee, A.A. Karande, A.R. Chakravarty, BODIPY appended copper(ii) complexes of curcumin showing mitochondria targeted remarkable photocytotoxicity in visible light, MedChemComm, 6 (2015) 846-851. https://doi.org/10.1039/C4MD00425F

[20] A. Bhattacharyya, A. Dixit, S. Banerjee, B. Roy, A. Kumar, A.A. Karande, A.R. Chakravarty, BODIPY appended copper(ii) complexes for cellular imaging and singlet oxygen mediated anticancer activity in visible light, RSC Advances, 6 (2016) 104474-104482. https://doi.org/10.1039/C6RA23118G

[21] N. Mukherjee, S. Podder, K. Mitra, S. Majumdar, D. Nandi, A.R. Chakravarty, Targeted photodynamic therapy in visible light using BODIPY-appended copper(ii) complexes of a vitamin B6 Schiff base, Dalton Trans., 47 (2018) 823-835. https://doi.org/10.1039/C7DT03976J

[22] Z. Zhu, X. Zhou, Y. Wang, L. Chi, D. Ruan, Y. Xuan, W. Cong, L. Jin, Fluorescent staining of glycoproteins in sodium dodecyl sulfate polyacrylamide gels by 4H-[1]-benzopyrano[4,3-b]thiophene-2-carboxylic acid hydrazide, Analyst, 139 (2014) 2764-2773. https://doi.org/10.1039/C3AN02309E

[23] R. Jovito, A. Neves, A.J. Bortoluzzi, M. Lanznaster, V. Drago, W. Haase, A new unsymmetrical dinucleating ligand and its first FeIIIZnII complex: Structure and solid state properties of an unexpected tetranuclear complex containing the [FeIII(μ-OH)2FeIII] structural motif, Inorg. Chem. Commun., 8 (2005) 323-327. https://doi.org/10.1016/j.inoche.2005.01.007

[24] L. Palatinus, G. Chapuis, SUPERFLIP - a computer program for the solution of crystal structures by charge flipping in arbitrary dimensions, J. Appl. Crystallogr., 40 (2007) 786-790. https://doi.org/10.1107/S0021889807029238

[25] G. Sheldrick, Crystal structure refinement with SHELXL, Acta Crystallogr. Sect. C, 71 (2015) 3-8. https://doi.org/10.1107/S2053229614024218

[26] O.V. Dolomanov, L.J. Bourhis, R.J. Gildea, J.A.K. Howard, H. Puschmann, OLEX2: a complete structure solution, refinement and analysis program, J. Appl. Crystallogr., 42 (2009) 339-341. https://doi.org/10.1107/S0021889808042726

[27] W. Qin, M. Baruah, W.M. De Borggraeve, N. Boens, Photophysical properties of an on/off fluorescent pH indicator excitable with visible light based on a borondipyrromethene-linked phenol, Journal of Photochemistry and Photobiology A: Chemistry, 183 (2006) 190-197. https://doi.org/10.1016/j.jphotochem.2006.03.015

[28] P. Ashokkumar, H. Weißhoff, W. Kraus, K. Rurack, Test-Strip-Based Fluorometric Detection of Fluoride in Aqueous Media with a BODIPY-Linked Hydrogen-Bonding Receptor, Angew. Chem. Int. Ed., 53 (2014) 2225-2229. https://doi.org/10.1002/anie.201307848

[29] R. Jovito, A. Neves, A.J. Bortoluzzi, M. Lanznaster, V. Drago, W. Haase, A new unsymmetrical dinucleating ligand and its first FeIIIZnII complex: Structure and solid state properties of an unexpected tetranuclear Fe2IIIZn2II complex containing the [FeIII(μ-OH)2FeIII] structural motif, Inorg. Chem. Commun., 8 (2005) 323-327. https://doi.org/10.1016/j.inoche.2005.01.007

[30] G. Palla, G. Predieri, P. Domiano, C. Vignali, W. Turner, Conformational behaviour and E/Z isomerization of N-acyl and N-aroylhydrazones, Tetrahedron, 42 (1986) 3649-3654. https://doi.org/10.1016/S0040-4020(01)87332-4

[31] B.-x. Shen, Y. Qian, Z.-q. Qi, C.-g. Lu, Q. Sun, X. Xia, Y.-p. Cui, Near-infrared BODIPY-based two-photon ClO− probe based on thiosemicarbazide desulfurization reaction: naked-eye detection and mitochondrial imaging, Journal of Materials Chemistry B, 5 (2017) 5854-5861. https://doi.org/10.1039/C7TB01344B

[32] W.J. Geary, The use of conductivity measurements in organic solvents for the characterisation of coordination compounds, Coord. Chem. Rev., 7 (1971) 81-122. https://doi.org/10.1016/S0010-8545(00)80009-0

[33] H. Lavanant, H. Virelizier, Y. Hoppilliard, Reduction of copper(II) complexes by electron capture in an electrospray ionization source, J. Am. Soc. Mass. Spectrom., 9 (1998) 1217-1221. https://doi.org/10.1021/jasms.8b01118

[34] A.C.D.M. Reis, M.C.R. Freitas, J.A.L.C. Resende, R. Diniz, N.A. Rey, Different coordination patterns for two related unsymmetrical compartmental ligands: crystal structures and IR analysis of [Cu(C21H21O2N3)(OH2)(ClO4)]ClO4·2H2O and [Zn2(C22H21O3N2)(C22H20O3N2)]ClO4, J. Coord. Chem., 67 (2014) 3067-3083. https://doi.org/10.1080/00958972.2014.958080

[35] A. Loudet, K. Burgess, BODIPY Dyes and Their Derivatives: Syntheses and Spectroscopic Properties, Chem. Rev., 107 (2007) 4891-4932. https://doi.org/10.1021/cr078381n

[36] G. Ulrich, R. Ziessel, A. Harriman, The chemistry of fluorescent bodipy dyes: versatility unsurpassed, Angew. Chem. Int. Ed. Engl., 47 (2008) 1184-1201. https://doi.org/10.1002/anie.200702070

[37] M. Castillo, S.L. Raut, S. Price, I. Bora, L.P. Jameson, C. Qiu, K.A. Schug, Z. Gryczynski, S.V. Dzyuba, Spectroscopic differentiation between monomeric and aggregated forms of BODIPY dyes: effect of 1,1-dichloroethane, RSC Advances, 6 (2016) 68705-68708. https://doi.org/10.1039/C6RA10833D